*Int. J. Electrochem. Sci.*, 8 **(2013)** 3229 - 3253

International Journal of
ELECTROCHEMICAL
SCIENCE
www.electrochemsci.org

# Biomass Fuels for Direct Carbon Fuel Cell with Solid Oxide Electrolyte

*Magdalena Dudek*[1], *Piotr Tomczyk*[1], *Robert Socha*[2], *Marek Skrzypkiewicz*[3], *Janusz Jewulski*[3]

[1] AGH-University of Science and Technology, Faculty of Fuels and Energy, 30-059 Cracow, Mickiewicza 30, Poland
[2] Jerzy Haber Institute of Catalysis and Surface Chemistry, Polish Academy of Sciences, Niezapominajek 8, 30-239 Cracow, Poland
[3]Institute of Power Engineering, Augustówka 8, Warsaw, Poland
[*]E-mail: potoczek@agh.edu.pl

*Received:* 12 January 2013 / *Accepted:* 15 February 2013 / *Published:* 1 March 2013

Direct carbon fuel cells with solid oxide electrolyte (DC-SOFC) has attracted growing attention recently as an efficient generator of electricity. Moreover, the DC-SOFC can be acknowledged to devices that take advantage of RES, provided it is fed with biomass fuel. In this work, the comprehensive studies performed for various types of DC-SOFCs supplied with charcoals and pyrolyzed in situ wood-chips are presented. Firstly, the samples of fuels were characterized by ultimate analysis, XRD, XPS spectroscopy and thermal analysis (DTA/DSC-TG). These studies showed that the charcoal samples had high carbon, low sulphur and very low ash contents. Although the analyses also confirmed the presence of graphite-like phase in the samples, their structure was highly defected and contained amorphous C. Then, the characteristics of small (2 $cm^2$), laboratory DCFCs fed with biomass fuels were determined and analyzed. On the basis of these measurements, the influences of structural, physical and chemical properties of fuels on the performance of fuel cells were evaluated. Five different types of fuels cells were used in these studies; they were constructed from the same solid electrolyte (8YSZ) and LSM-GDC composite cathode but varied in material of anode. The tests performed with these fuel cells showed that: (1) charcoals are suitable and attractive fuels for the DC-SOFC providing sufficiently high power density and (2) one of the possible ways of improving the DCFC parameters is the application of new anode materials which are good catalysts for the Boudouard reaction and resistant against possible chemical degradation. Results of tests with larger DCFCs of dimensions 5 cm x 5 cm fed with charcoal fuel are also presented in the article.

**Keywords:** biomass, carbon, solid oxide fuel cell, direct carbon fuel cell,

## 1. INTRODUCTION

Biomass is one of the most important energy carriers among the RES. However, it has still unappreciated position in comparison to wind and solar energy despite its undisputed advantage – it

can be used at any arbitrary time to produce energy [1-3]. Unfortunately, using biomass as a fuel in thermal power plants is often economically unjustified due to low efficiency of conversion to electricity and high costs of transportation [4-6]. Higher efficiency of conversion can be reached in fuel cells, however, this technology requires an additional processing step, namely gasification, which produces fuel that is rich in hydrogen. The endothermic process of gasification consumes a part of biomass feed in the gasifier reactor, causing a loss of over 20% of energy in comparison to its primary amount [7-9].

Development of the direct carbon fuel cell (DCFC) opens new opportunities to convert various carbonaceous fuels to electricity. The DCFCs can be fed with a large number of carbon-rich fuels but biomass and organic waste are at the center of attention because they are renewable and can be processed into pure carbon fuel. As a fuel, charcoal produced from biomass and waste has many benefits:

- is inexpensive to produce and easy to store;
- is readily available to consumers worldwide from compacted beds with high-energy density particles;
- has no mercury, almost no sulphur, low nitrogen and produces very little ash when burned; has high electrical conductivity, a large surface area and many bonds that makes it very reactive at relatively modest temperatures [10,11].

Charcoal is a product of wood burning in an oxygen poor atmosphere. Significant chemical changes take place in the plant material during the charring process. As the temperature increases the major structural components of the wood (hemicellulose, cellulose and lignin) break down while CO, $CO_2$ and other gases are released [12]. The evaporation of this gases results in condensation of the carbon skeleton and aromatization, which leads to the formation of graphite – like layers. Organic compounds with higher proportions of aromatic compounds have higher char yields that implies that graphite-like layers are formed in larger amounts.

The overall process of producing electricity from biomass in a DCFC gains efficiency by its simplicity. It involves only two steps: (1) drying (and/or pyrolysis or hydrothermal carbonization) to obtain char and (2) directly feeding the DCFC with produced fuel [13,14].

Various types of DCFCs have been investigated recently. One of the most popular classifications regards a type of electrolyte used in the cell: alkaline, molten carbonates or solid oxide [15,16]. In 1988, Ishida et al. [17] demonstrated the feasibility of a direct carbon fuel cell with solid oxide electrolyte (DC-SOFC), i.e. without any liquid material. They anticipated that $CO_2$ was a final product of carbon oxidation at the anode of this cell, formed in a sequence of the following electrochemical reactions:

$$C + O^{2-} \rightarrow CO + 2e^{-} \quad (1)$$

$$CO + O^{2-} \rightarrow CO_2 + 2e^{-} \quad (2)$$

The Boudouard reaction (3), involving $CO_2$ and C as reactants, was an additional source of CO consumed in reaction (2):

$$C + CO_2 \rightarrow 2CO \quad (3)$$

The direct carbon fuel cell with solid oxide electrolyte is believed to be the most promising type of DCFCs, due to its uncomplicated maintenance and on-going progress in material development. Apart from biomass fuels, the DC-SOFC is suitable for utilization of waste carbonaceous products as medium density fiberboard (MDF), carbon-waste product of methane plasma splitting and organic and plastic wastes, which are detrimental to the environment and sometimes difficult to recycle [18,19]. However, further development and commercialization of the DC-SOFC require significant improvements in the fuel utilization and efficiency of direct conversion of carbon fuels into electricity [20].

The aim of this paper is to examine possible utilization of different fuels derived from biomass in the DC-SOFC. Special emphasis is put on relation between properties of charcoal-based fuels and characteristics of the DC-SOFC. The effect of anode materials on performance of the DC-SOFC is also discussed.

## 2. EXPERIMENTAL

Three different types of carbon fuels derived from wood biomass were investigated:

- Charcoal, (carbon powder, supplied by Merck Germany), noted hereafter as Charcoal A;
- Carbo medicinalis (commercial product supplied by Gryfskand, Poland), noted hereafter as Charcoal B.
- Wood-chips produced from a beech wood and pyrolysed in situ in the DC-SOFC, noted hereafter as Charcoal C

### *2.1. Analytical methods for characterization of charcoal fuels*

The phase compositions of all the charcoal samples were evaluated by X-ray diffraction analysis referring to the ICDD database. The XRD measurements were done using the Panalytical X'Pert Pro system with monochromatic $CuK_\alpha$ radiation. The contents of elements such as carbon (C), nitrogen (N), sulphur (S) and hydrogen (H) in all the investigated samples were determined with a 2400 CHN Elemental Analyzer Perkin Elmer. Specific surface area was measured using multipoint nitrogen adsorption at -196$^{O}$C (Quantachrome Pore Master). A scanning electron microscopy (Nova NanoSEM) coupled with an EDS system was used to characterize the morphology and chemical composition of the carbon particles. Thermal effects occurring during heating of the solid carbon fuel in the temperature range 25-1000$^{O}$C in argon gas flow were measured by the DTA/DSC and TG methods (SDT 2960 TA Instruments). Chemical surface analyses of the carbon fuels were performed by a XPS/ESCA method with a hemispherical analyzer (SES R 4000, Gammadata Scienta). The spectra were processed using Casa XPS 2.3.12 software, while the background was estimated by a Shirley profile. The spectra deconvolution into a minimum number of components was done by an application of Voigt-type line shapes. The chemical reactivity of nickel particles vs. carbon particles

was conducted on pellets consisting of 1 : 1 weight ratio mixture of metal and carbon powders and heated at 700-900$^{o}$C for 12 h in Ar or $CO_2$ – gas atmospheres. Following the tests, the mixtures were also characterized by the XRD diffraction method.

### *2.2. Electrochemical measurements*

The electrochemical oxidation of carbon was studied using five types of small solid oxide fuel cells (button-size with ca. 2 cm$^2$ active surface area) with the same electrolyte (8YSZ) and cathode (LSM-GDC) materials, which varied only in composition of anode material:

(a) C|Ni-YSZ|8YSZ|LSM-GDC|LSM|$O_2$
(b) C|Ni-GDC|8YSZ|LSM-GDC|LSM|$O_2$
(c) C|($Ni_{0.9}$-$Fe_{0.1}$)-GDC|8YSZ|LSM-GDC|LSM|$O_2$
(d) C|LCCr|8YSZ|LSM-GDC|LSM|$O_2$
(e) C|8YSZ|LSM-GDC|LSM|$O_2$

where: 8YSZ was an electrolyte consisting of 8 mol.% $Y_2O_3$ in $ZrO_2$, LSM was a $La_{0.8}Sr_{0.2}MnO_3$ porous cathode material deposited by screen printing, LSM-GDC was a composite cathode material consisting of LSM+10 mol.% $Gd_2O_3$ in $CeO_2$ (GDC), Ni-YSZ, Ni-GDC and ($Ni_{0.9}$-$Fe_{0.1}$)-GDC and $La_{0.8}Ca_{0.1}Sr_{0.1}CrO_3$ (LCCr) were used as anode materials.

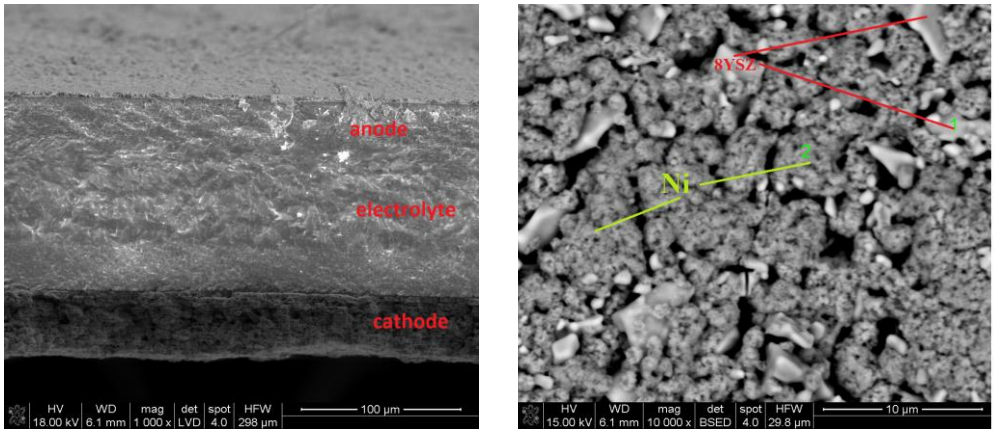


**A** **B**

**Figure 1**. a)Cross section of Ni-YSZ|8YSZ|LSM-GDC|LSM solid bottom oxide fuel cell; b)Surface of Ni-YSZ anode

The thickness of the electrolyte, anode and cathode were ~160, 50 and 52 μm respectively. Typical SEM images of cross section of type (a) DC-SOFC, cross section of interface 8YSZ/LSM-GDC/LSM and surface of Ni-YSZ anode material before the electrochemical tests are presented in Fig.1a –b.

Apart from the cermetallic materials, initial investigations with the DCFC equipped with an anode made of oxide perovskite were also done. In this work $La_{0.8}Ca_{0.1}Sr_{0.1}CrO_3$ (LCCr) with mixed ionic-electronic conductivity (MIEC) was chosen for the tests. The majority of the tests, reported in the literature [21-23], were performed with small, button-size DC-SOFCs. Therefore, the results of our measurements can easily be compared to the data obtained by the other authors. However, we have also performed few experiments with larger cells, namely square shaped DC-SOFCs of dimensions 5 cm x 5 cm. The purpose of these experiments was to examine the effect of the system scaling-up. The experimental set-up for testing the button-size DC-SOFC was described in our previous paper [24]. Electrochemical measurements were performed in the temperature range of 500-800$^{o}$C, using a potentiostat PGSTAT 300N equipped with GPES (chrono- and pulse techniques) and FRA (electrochemical impedance spectroscopy) modules. Before and after the tests, the surface of electrode materials and cross–section of the fuel cells were examined by a scanning electron microscope.

## 3. RESULTS AND DISCUSSION

### *3.1. Analytical evaluation of charcoal samples*

Different types of biomass vary in relative amounts of cellulose, hemicellulose, lignin and inorganic compounds that affect their volatility, ash content and other physicochemical properties. In the DC-SOFC fed directly with biomass, the feed undergoes pyrolysis process, i.e. thermal decomposition of organic substances in the absence of oxygen, which results in production of charcoal, liquid and gaseous products. Depending on the applied thermal conditions (temperature and heating rate), one can obtain liquid, solid and gaseous products in required proportions.

Firstly, the properties of biomass fuel were determined by ultimate analysis. The concentrations of major elements in three charcoals samples under studies are collected in Table 1.

**Table 1.** Concentrations (wt.%) of major elements in the charcoal samples

| Sample | C | H | S |
|---|---|---|---|
| Charcoal A | 93.1 | 0.54 | 0.02 |
| Charcoal B | 94.6 | 0.49 | 0.04 |
| Charcoal C | 84.3 | 0.35 | --- |

The data presented in Table 1 show that amounts of carbon, hydrogen and sulphur are very similar in all the investigated samples of charcoals. High carbon, low sulphur and very low ash contents (below 1% in all the samples) are generally typical for most charcoals. The fuel with high content of carbon and low content of contaminations is very favorable for efficient and failure-free operation of the DC-SOFC. The data in Table 1 also indicates that it is possible to obtain valuable solid carbon fuel from wood-chips produced from a beech wood and pyrolyzed in situ in the DC-SOFC (Charcoal C).

The XPS analysis allowed us to determine atomic compositions and electronic properties of the elements present at the surface of charcoal particles. The analysis was performed for the surface layer up to the depth of 10.3 nm. The data obtained is presented in Table 2.

**Table 2.** The elemental compositions at the surfaces of Charcoals A and B particles determined by the XPS method.

| Sample | | Atomic concentration (at.%) | | | |
|---|---|---|---|---|---|
| | C 1s | O 1s | S 2p | Si 2p | Mg |
| Charcoal A | 88.2 | 8.3 | 0.1 | 2.5 | 0.9 |
| Charcoal B | 94.0 | 5.9 | 0.1 | ---- | ---- |

**Table 3.** The parameters of the deconvoluted C 1s and O 1s spectra for Charcoals A and B.

| Component | Charcoal A | | Charcoal B | | Assignation |
|---|---|---|---|---|---|
| | BE (eV) | % | BE (eV) | % | |
| C 1s core excitation | | | | | |
| A | 283.9 | 77.2 | 284.1 | 84.9 | C-C $sp^2$ |
| B | 285.9 | 5.4 | 285.3 | 8.1 | C-C $sp^3$ |
| C | 286.5 | 8.4 | 287.3 | 2.5 | C=O |
| D | 288.0 | 5.6 | 288.8 | 2.2 | COOH |
| E | 289.7 | 1.9 | 290.1 | 2.3 | $CO_3^{2-}$ |
| X | 282.7 | 1.6 | - | - | carbides |
| A'-A'''' | 288.3-292.9 | - | 288.5-293.7 | - | plasmon and dipole excitation satellites |
| O 1s core excitation | | | | | |
| A | 530.7 | 27.7 | 530.9 | 33.1 | OH, C-O-C, $CO_3^{2-}$ |
| B | 532.5 | 42.6 | 532.9 | 66.9 | $H_2O$ + $O^{2-}$ in aliphatic compounds |
| C | 534.2 | 29.7 | - | - | $O^{2-}$ in aromatic compounds |
| sat | 536.2 | - | 536.8 | - | shake-up |

As can be seen in Table 2, the oxygen to carbon ratio was equal to 0.094 and 0.063 for Charcoals A and B respectively, meaning that surface oxidation of Charcoal A was higher than that of

Charcoal B. On the contrary to Charcoal B, small amounts of silica and magnesium were detected at the surface of Charcoal A particles - in the case of Si in form of silica (binding energy, BE Si $2p_{3/2}$ = 103.2 eV) [25,26]. Both the carbon samples also contained traces of sulphur in the surface layer. The detailed analysis of high resolution C 1s spectra for both the charcoal samples is presented in Fig.2 and Table 3. The C 1s spectra were deconvoluted in accordance with the procedure described by Leiro et al. [27]. The C 1s core excitation shows very similar spectrum envelopes for both the studied samples of Charcoals A and B. Each spectrum was deconvoluted into five components assigned to specific carbon species and five satellites ascribed to plasmon and dipole excitations.

The data reported in Table 2 confirmed that the oxidation of Charcoal A was higher than Charcoal B, i.e. the overall contributions of oxidized carbon species in Charcoals A and B were equal to 15.9% and 7.0%, respectively. Additionally, the deconvolution of the C 1s spectrum allowed us to estimate the ratio of $sp^2$ to $sp^3$ forms of carbon [25-27]. They were equal to 14.2 and 10.5 for Charcoals A and B respectively, indicating larger amounts of graphite-like carbon in Charcoal A. The O 1s spectra (Fig.2) were deconvoluted into components assigned to oxygen in hydroxyl, ether and carbonate groups (A component) or oxygen in water or aliphatic compounds (B component) or oxygen in aromatic compounds (C component) (Table 2) [25]. The component with the binding energy of about 536 eV was assigned to shake-up satellites of $\pi^*$ electrons. The C component was not observed in the O 1s spectrum of Charcoal B which suggested that oxidation of graphite-like carbon lattice was higher at the surface of Charcoal A particles.

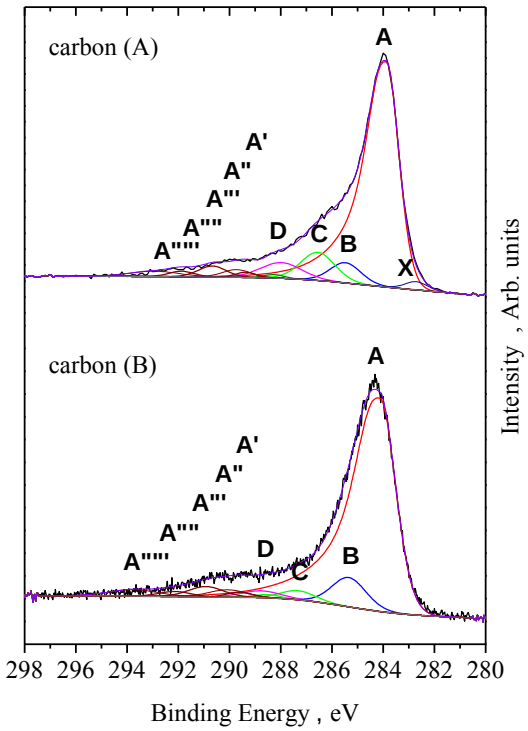


**Figure 2.** The XPS detailed analysis of high resolution C 1s spectra for Charcoal A and B samples.

It is worth noticing that the O 1s line corresponds to a nonspecific excitation, where several components can show similar BE at the maximum of photoelectron spectrum. It can be also postulated

that the responses attributed to the oxygen components are related to the presence of adsorbed water in the samples of Charcoals A and B, which is higher in the latter as determined from the independent analysis of moisture content (8.3 and 10 %, respectively).

The X-ray diffraction patterns recorded for all the investigated carbon samples are presented in Fig.3.

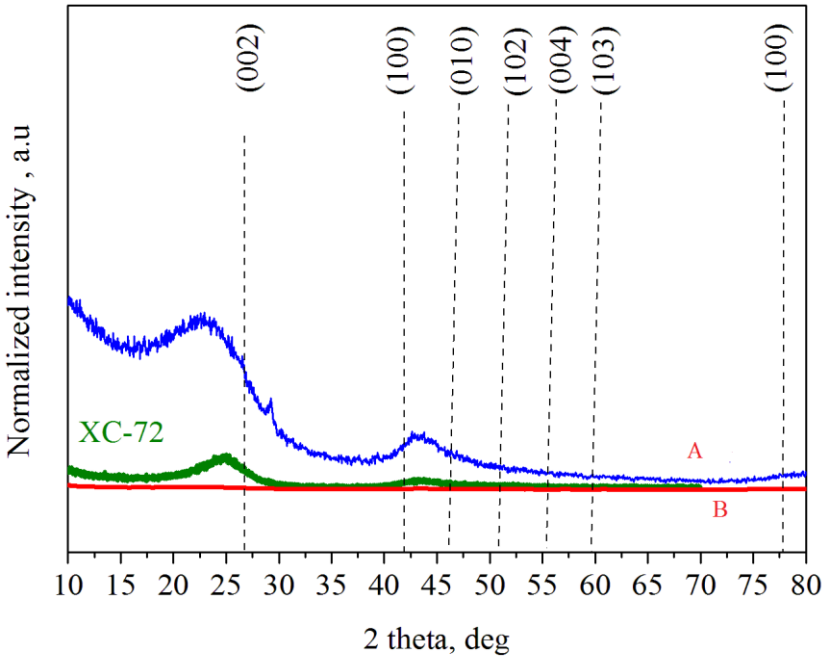


**Figure 3.** X-ray diffraction patterns recorded for Charcoals A and B samples. Vertical lines correspond to the peak positions of graphite. For comparison data for commercial carbon powder Cabot XC-72 was also added.

The XRD spectra were normalized towards the peak at $2\theta$ = 20-26 deg. The vertical lines mark the position of the peaks corresponding to the tabulated graphite diffraction patterns. The patterns presented in Fig.3 are rather typical for a disordered carbon phase [28]. However, the XRD patterns of both Charcoals A and B also show the response, which likely can be attributed to a short range graphite structure [29,30] – if it is so, Charcoal A contains more graphite-ordered particles in comparison to Charcoal B.

Besides the phase composition, active surface area of fuel may also affect the performance of carbon oxidation in the DC-SOFC. The surface areas of Charcoal A and B powders were determined to be 728.6 and 1249 $m^2/g$, respectively. Charcoal C, formed in situ by pyrolysis of wood chips, had the surface area equal to 543.8 $m^2/g$.

Typical SEM microphotographs of Charcoals A and B powders are presented in Fig. 4a-b Charcoal A consisted mainly of isolated spherical porous particles of diameter 0.5 to 20 μm, some agglomerates of size 20 to 40 μm were also observed. In the case of Charcoal B, the shape of the carbon particle was spherical or oblong (elongated) and their sizes varied from 0.5 to 25 μm.

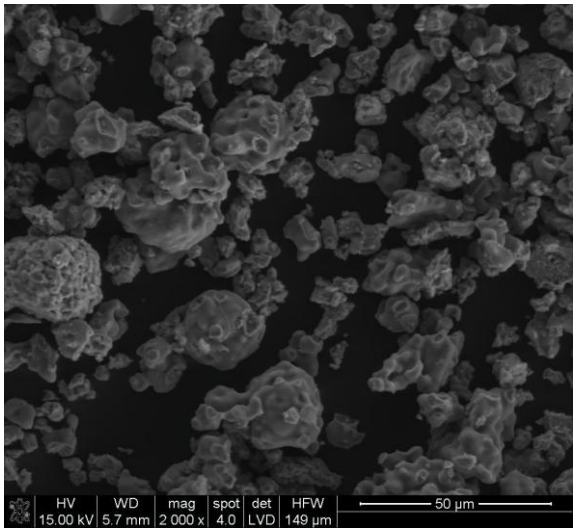


Charcoal A (a),

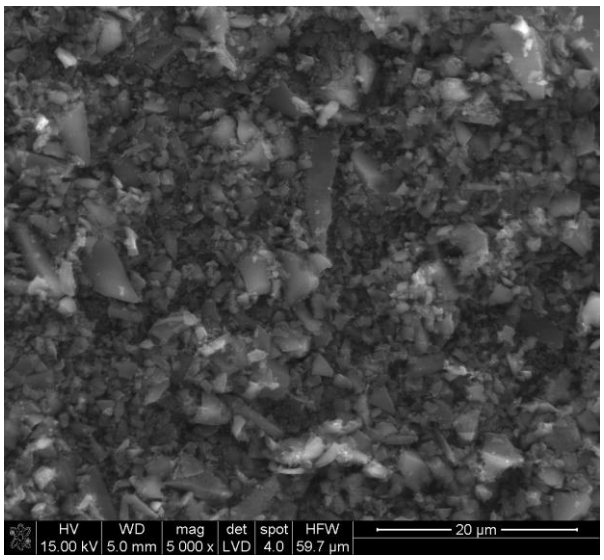


Charcoal B - Carbo–medicinalis (b)

**Figure 4.a –b** SEM microphotographs of the investigated charcoal samples:

The thermal analysis of the samples were performed to elucidate the thermal and chemical stabilities of the charcoal fuels at the temperatures of the DC-SOFC operation, i.e. 600-1000$^{o}$C. The samples (ca. 50 mg), placed in an alumina crucible, were ramped–up at 10 K·min$^{-1}$ rate. $CO_2$, a final product of C oxidation in the cell (equation 2) protected carbonaceous fuels from direct reaction with the environmental air. Apart from $CO_2$, also $N_2$, Ar and gas mixtures of Ar + $CO_2$ were used as shielding gases, especially when kinetics and mechanism of the electrode reactions were studied. The typical thermal effects observed in the DTA/DSC and TG experiments with Charcoals A and B are presented in Fig 5a -b.

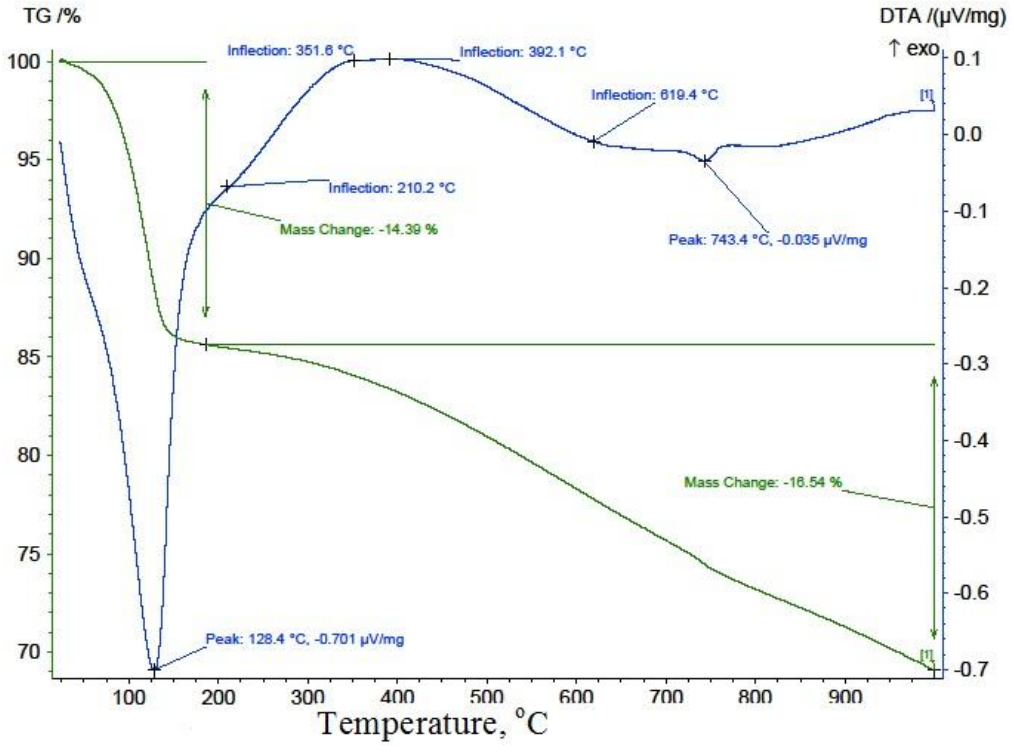


Charcoal A (a),

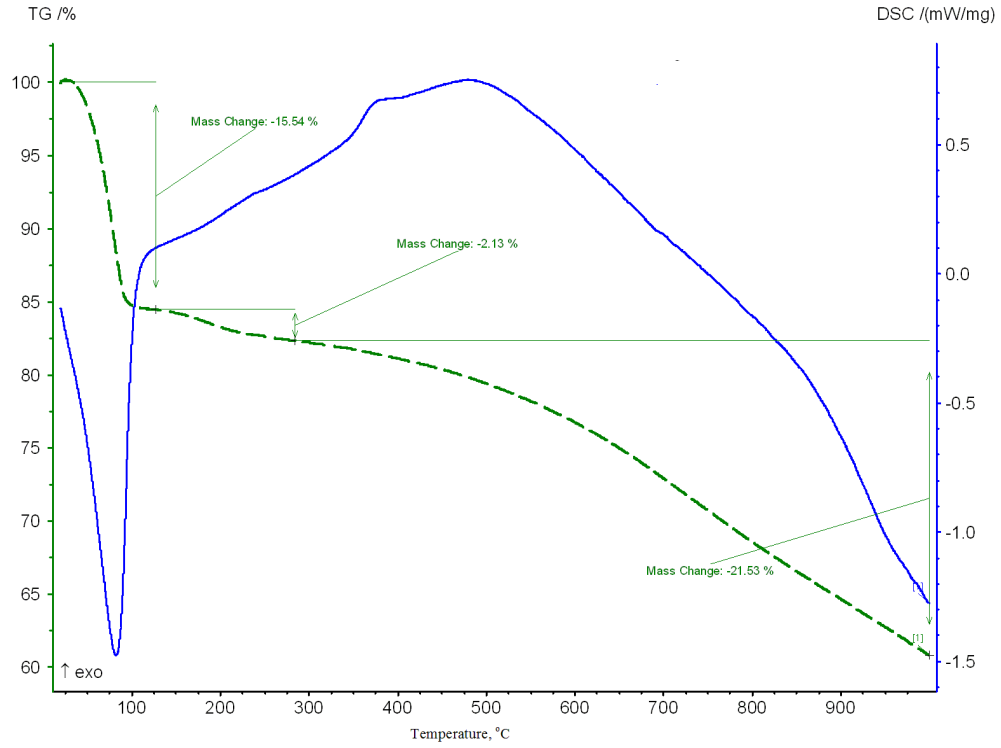


Charcoal B - Carbo–medicinalis (b)

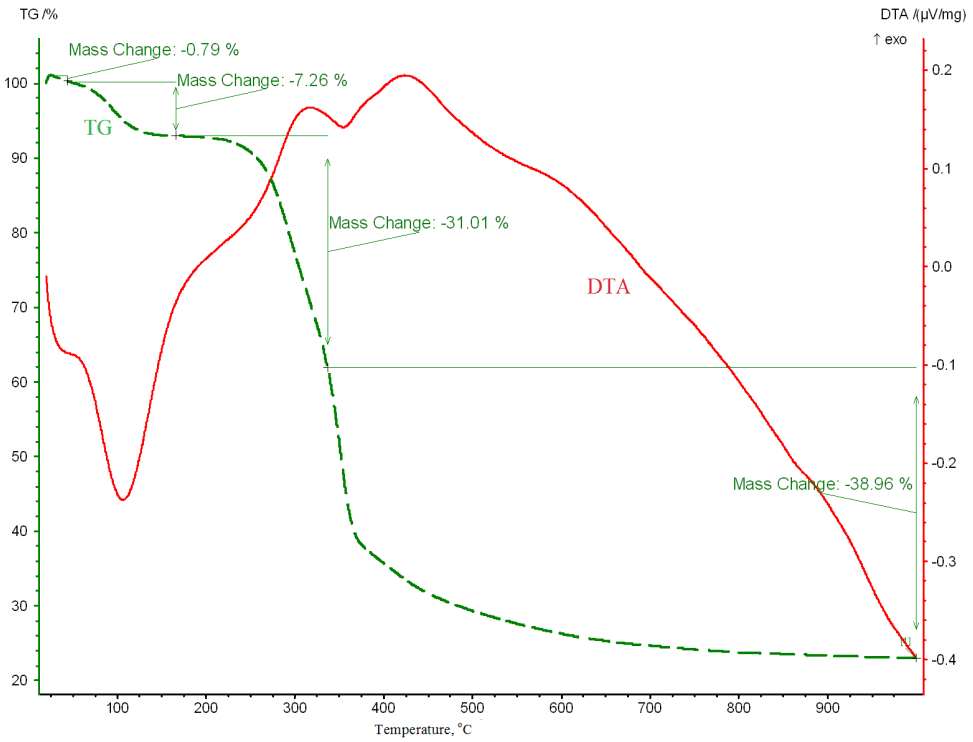


Charcoal C - wood-chips pyrolysed in situ (c).

**Figure 5.** a–c The TG/DSC and DTA-TG curves recorded for the investigated charcoal samples: Charcoal A (a), Charcoal B - Carbo–medicinalis (b) and Charcoal C - wood-chips pyrolysed in situ (c).

When the samples were heated from 25 to 1000$^{O}$C under argon atmosphere, the TG curves showed two regions of mass losses for both the charcoal samples investigated. The overall mass losses of ca. 15 % for Charcoal A and ca. 18 % for Charcoal B were observed in the low temperature region (25-300$^{O}$C). They could be attributed to the evaporation of adsorbed water and decomposition of organic substances. In the case of the temperature range 300-1000$^{O}$C, the mass losses of ca 16 % and 22 % were recorded and could be connected with further evaporation of adsorbed gases and pyrolysis. The processes attributed to charcoal pyrolysis occurred at higher temperatures (500-1000°C). The analysis of the data indicated that there is no phase/structural changes of charcoal fuels in the temperature range of 750-1000°C, i.e. at the operating temperatures of the DC-SOFC. The DTA/TG curves were also detected for wood-chips (Fig. 5c).

In the case of this sample, the losses of mass of about 30 % was detected in the low temperature range of 25 to 300$^{O}$C, but in the higher temperature range of 400-1000$^{O}$C the mass losses were analyzed for 33 % of total mass of samples. Some thermal effects were detected in the temperature range of 300-500$^{O}$C which originated from pyrolysed samples. After temperatures higher than 600$^{o}$C no thermal effects corresponding to phase changes were observed. The mass losses of all samples were considered to calculate the adequate mass of solid fuel for DC-SOFC tests. The amount of carbon powder also has influence on the DC-SOFC's performance.

*3.2. Chemical reactivity of carbon particles with components of Ni-YSZ cermetallic anode materials*

The state-of-the-art planar and tubular DC-SOFCs are built from ceramic components, which are frequently applied in solid oxide fuel cells fed with hydrogen ($H_2$-SOFC). In the case of cathode, this practice is justified by the fact that the same electrode reaction of oxygen reduction occurs in both types of fuel cells, i.e. the DC-SOFC and $H_2$-SOFC. However, in the case of anode, the electrode reactions are different in the DC-SOFC and $H_2$-SOFC, at least because of different fuels, which are in direct contact with the electrode (C, CO and $H_2$, respectively).

A Ni-YSZ cermet is commonly used as an anode material in the $H_2$-SOFC, due to its good electrocatalytic properties, mechanical and chemical stabilities, proper thermal behavior and high electric conductivity. Nevertheless, it is enough to supply a solid oxide fuel cell with a natural gas and the Ni-YSZ-based anode suffers from many drawbacks, for example, notable sulfur poisoning and carbon deposition resulting from methane cracking [31-33]. In the DC-SOFC, iron, nickel, cobalt and alloys based on these metals may corrode in direct contact with highly active carbon at high temperatures (300-850°C). This process leads to disintegration of bulk metals and alloys into metal particles and is known as metal dusting. The rate of Ni corrosion depends on the temperature and gas composition [34,35].

T. Horita et al. [36] found that at temperatures above 900$^{o}$C, nickel carbide $Ni_3C$ can be formed as a product of reaction between nickel and graphite. The impact of $Ni_3C$ formation on the performance of DC-SOFC has not been thoroughly explained as yet. It is likely, due to low melting temperature and tendency to coagulate, that $Ni_3C$ hinders contact between C particles and YSZ electrolyte . On the other hand, T. Gür et al. [37] reported that carbides of titanium, vanadium and zirconium are promising catalysts, which accelerate electrochemical oxidation of carbon and increase current and power densities acquired from the DC-SOFC. Pellets made of nickel and carbon (Charcoal A or Charcoal B) mixture were heated at 700, 750, 800 and 850$^{o}$C for 12 h. After cooling the samples were investigated with the XRD (Fig. 6a-b)

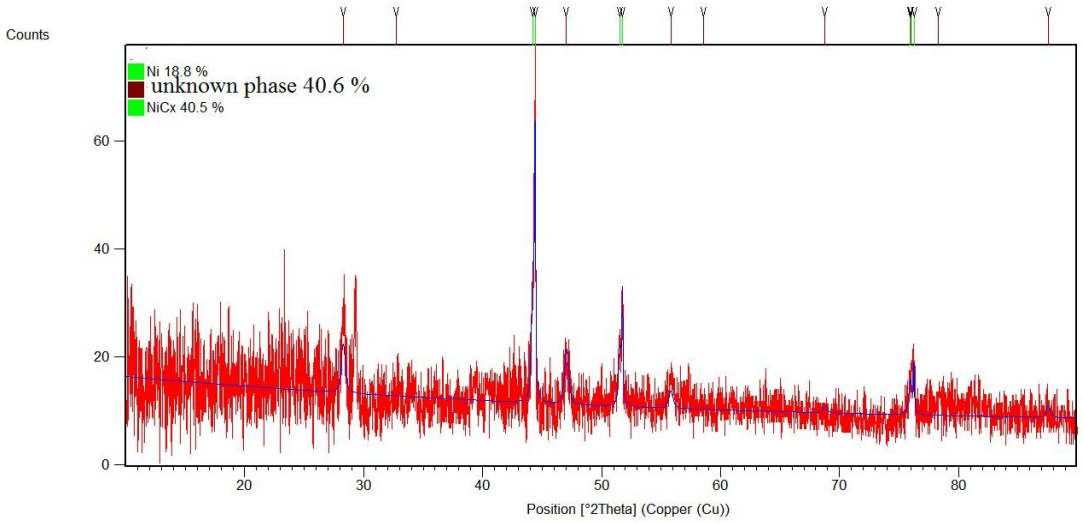


**Figure 6. a)** The X-ray diffraction patterns of mixture of Charcoal A powder and nickel after common heating at temperature 850$^{o}$C. in Ar gas atmosphere

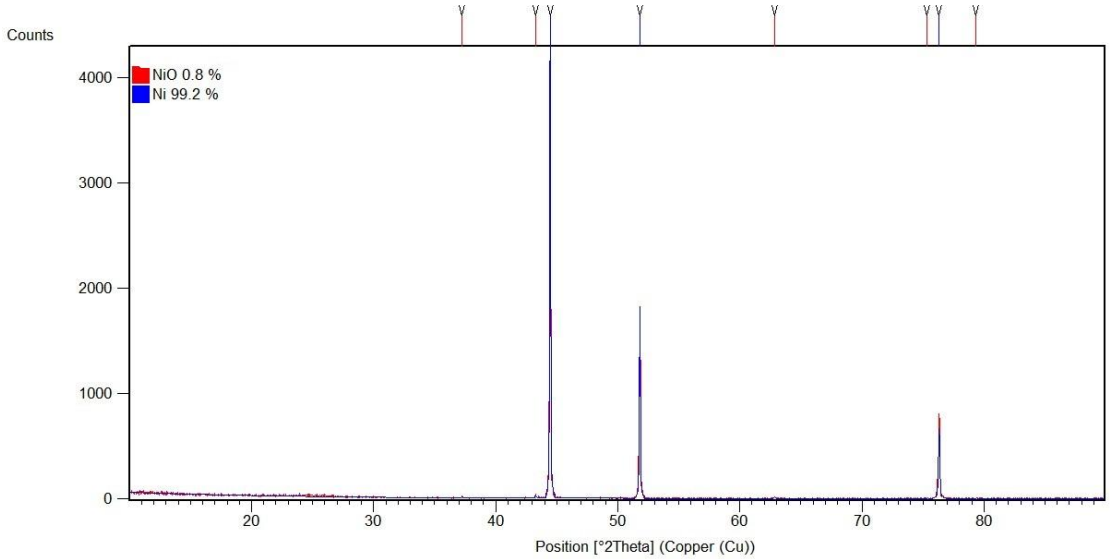


**Figure 6. b)** The X-ray diffraction patterns of mixture of Charcoal A powder and nickel after heating at temperature 850$^{o}$C. in $CO_2$ gas atmosphere

The XRD pattern of the pellet heated at 850$^{o}$C in argon flow gas revealed the presence of very small amounts of nonstoichiometric phase $Ni_xC$ and of unknown phase as a product of undesirable reaction (Fig.6a). This observation is in rather good agreement with the conclusion of T. Horita which postulate possible formation of nickel carbide ($Ni_3C$) in the conditions of the DC-SOFC operation. To explain how this phenomenon affects the performance of the fuel cell, additional investigations are required, especially these performed in long durations of DC-SOFC operating. The Fig 6b. presents the X-ray diffraction pattern recorded for sample (mixture Ni and C) heated at the same conditions but under $CO_2$ gas flow. In this case only Ni and impurities of NiO phase were observed. These results clearly showed that further investigations of chemical stability of the Ni-YSZ anode in contact with carbon powder during conditions typical for operating the DC-SOFC are required.

### *3.3. Electrochemical investigations*

#### *3.3.1. Mechanism of carbon electro-oxidation in the DC-SOFC*

In the DC-SOFC, carbon fuel can be oxidized directly ($C + O^{2-} \rightarrow CO_2 + 4e^-$)- reaction 4 or indirectly (reactions 1-3). The direct oxidation of carbon occurs at contact points between C particles and carrier of oxide ions, i.e. solid oxide electrolyte and/or MIEC (mixed ionic-electronic conductor) anode. Although most of the experiments with the DC-SOFC have been done for the cells of analogous construction to a typical $H_2$-SOFC, reaction (4) may also take place at a "bare" oxide electrolyte, which is not covered with any anodic material.

However, in such a "half-cell", the oxidation of CO, product of reactions 1 and 3, proceeds with very low intensity, because: (i) electro-oxidation of carbon monoxide (reaction 2) occurs only at the contact points between C, CO and oxide electrolyte and (ii) carbon is not a good electro-catalyst of

reaction 2. When oxide electrolyte is coated with porous MIEC anode, reaction 2 occurs at the whole, very large active area of the electrode that results in enlargement of current produced during the cell loading. In the specific case of supplying the (a) type DC-SOFC with carbon formed by $CH_4$ splitting, C fuel distributes over the whole surface of the Ni-YSZ cermet anode, although has a tendency to stick mainly to its Ni-rich areas in the form of superficial agglomerates. According to Li et al. [38], the deposited carbon can be directly electro-oxidized during loading, independently of the location at the electrode. Regarding carbon located at YSZ-rich areas of the anode, reaction 1 occurs with carbon reactive site (CRS) and involves $O^{2-}$ ions acquired from the ionic conductor while released $e^-$ is conducted throughout the deposited carbon to an external circuit. When carbon is placed at the Ni-rich areas, $O^{2-}$ ion from the YSZ is electrochemically forced onto the Ni surface via the polarized metal-electrolyte interfaces, where it releases $e^-$ to form $O^-$. Then $O^-$ reacts with the carbon deposited on the Ni surface and electrons are conducted through the Ni particles outside. Most readily, the electro-oxidation of carbon occurs at the Ni-YSZ boundaries in the cermet electrode because $O^{2-}$ ions are freely available from the YSZ electrolyte, and released electrons can be easy transported through the percolation path of Ni and well conducted carbon.

Gür [39] proposes "CO shuttle mechanism" to explain the operation and behavior of several types of DCFCs under $CO_2$ and inert gas atmospheres. He suggests that oxygen adsorbed on the carbon surface desorbs as CO and subsequently undergoes electrochemical oxidation to $CO_2$ at the anode of the DC-SOFC. $CO_2$, formed this way, diffuses out the electrode to a carbon load and participates in the Boudouard reaction 3 to generate additional CO. The newly formed CO diffuses back to the anode, where it is electrochemically oxidized to $CO_2$, starting the cycle again.

### *3.3.2. Examination of various types of the DC-SOFC*

Typical dependencies of voltage ($\Delta E$) vs. current density ($I$) and power density ($P$) vs. current density ($I$) at various operating temperatures for the type (a) DC-SOFC with the Ni-YSZ cermetallic anode is shown in Fig.7. The $\Delta E$ vs. $I$ characteristics of the fuel cell were determined using a slow cyclic linear voltammetry method at the scan rate $v$ = 5 mV/s. These experiments were performed under flow of argon, which was supplied to the anodic compartment of the cell. The current and power densities were determined using the geometric area of anode for the fuel cell of planar geometry.

As can be seen, the open circuit voltage (OCV) of the cell increases with the temperature, approaching ca. 1.02 V at 800ºC. This voltage is close to the reversible voltage of carbon oxidation reaction vs. the oxygen electrode. Although there is no significant difference between curves shown in Figs.8a and 8b, the voltages at a given current density for the cell supplied with Charcoal B are slightly, but systematically, higher than those for the cell supplied with Charcoal A. This effect should not be exclusively attributed to the higher content of carbon and/or larger surface area of Charcoal B than Charcoal A. Since the ordered graphite–phase oxidizes slower than, for example, amorphous carbon, its lower concentration in Charcoal B can also be favourable for the better performance of the DC-SOFC. The useful criterion of the fuel cell quality is its maximum power density, $P_{max}$. For the DC-SOFCs supplied with Charcoals A and B, these $P_{max}$ were relatively high at 800°C and equal to

54 and 70 mW/cm$^2$ respectively. Frequently, the power density of single PAFC or MCFC in a prototype of stationary generator does not exceed 100 mW/cm$^2$ [40]

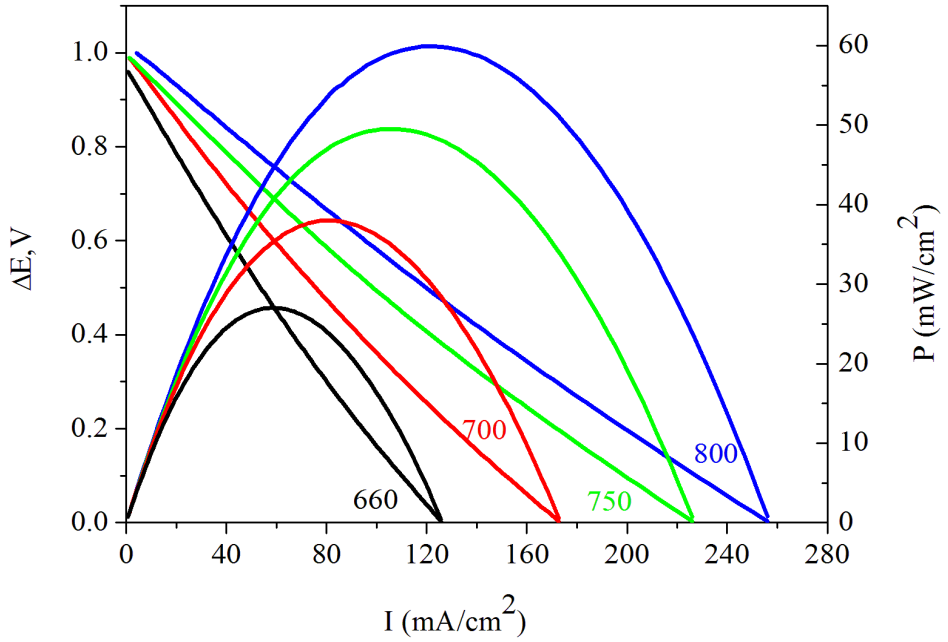


**Figure 7a.** Families of dependences: the cell voltage Δ*E* vs. the current density *I* and the power density *P* vs. *I* recorded for the 2 cm$^2$ DC-SOFC with Ni-YSZ anode fed with Charcoal (A )

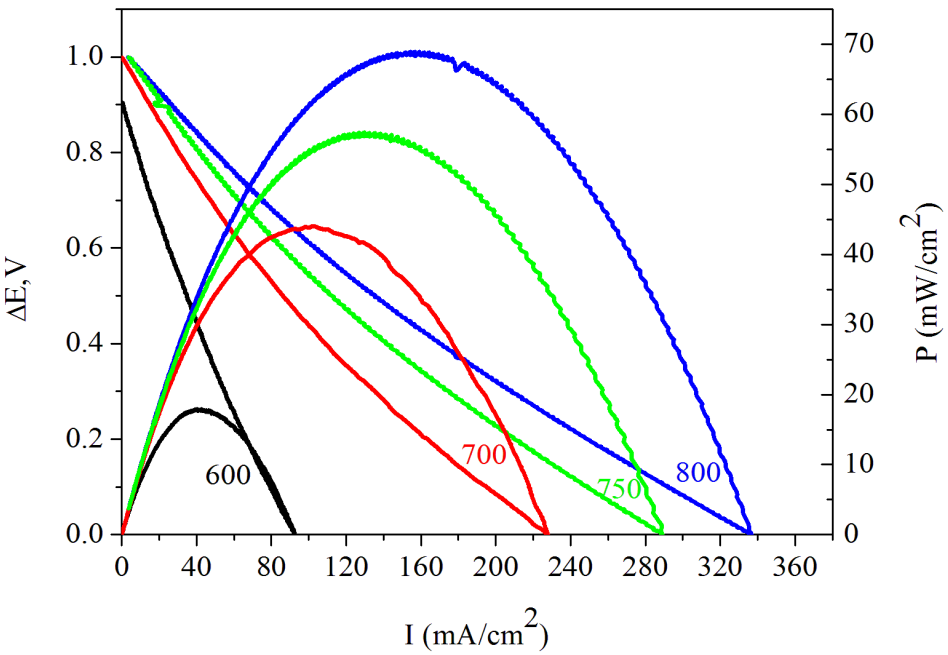


**Figure 7b.** Families of dependences: the cell voltage Δ*E* vs. the current density *I* and the power density *P* vs. *I* recorded for the 2 cm$^2$ DC-SOFC with Ni-YSZ anode fed with Charcoal B

Considering further, feasible development of the DC-SOFC, the obtained results show that carbon fuels produced on the basis of biomass can be suitable and useful fuel for this kind of fuel cell. To verify a reliability of the data obtained with the small fuel cells using scaling-up methodology, we determined the characteristics of the larger DC-SOFC of dimensions 5 cm x 5 cm (13cm$^2$ active area ) fed with Carbon A. They are presented in Fig.8. The conditions of experiments were the same as previously for the 2 cm$^2$ fuel cells, but different methodology of measurements was employed: the 13cm$^2$ fuel cell was loaded with the step-wise increasing current, each step was followed by 1 minute voltage stabilization. The maximum power density $P_{max}$ = 54 mW/cm$^2$ was determined at 800°C. This value was practically the same compared to the DC-SOFC of small dimensions (Fig.7a). In the consecutive experiment, a 12 hour long stability test was completed with the constant electric current load of 47 mA/cm$^2$. The determined polarization characteristic of the fuel cell is presented in Fig.9. A linear decrease in cell voltage (3.58 mV/h) was observed during the 12 hour test. The area specific resistance (ASR) calculated regarding the linear part of the polarization curve (0.5 - 0.8 V) increased from 4.4 Ω cm$^2$ to 5.4 Ω cm$^2$ during the test. It is worth noting the electrochemical data according to planar DC-SOFC with higher dimensions are rather limited in literature. Therefore comparative measurements performed for the DC-SOFC built from the same components seem to be valuable results for further developing DC-SOFC technology.

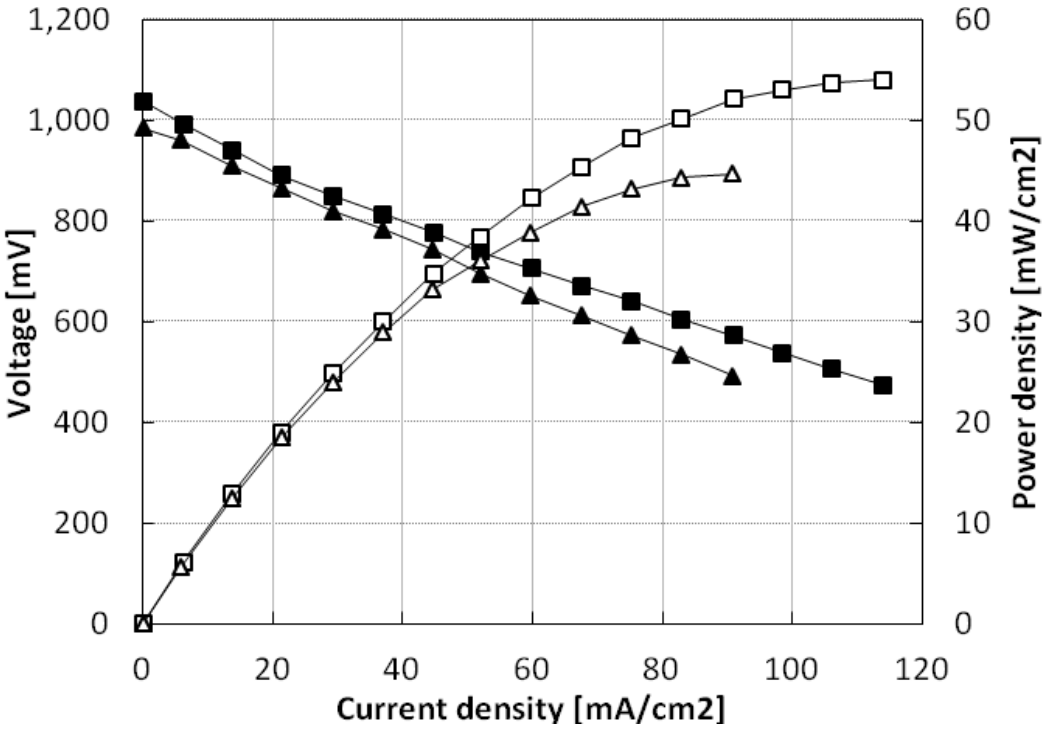


**Figure 8.** Curve V-I (black markers) and power density (white markers) characteristics of the direct carbon SOFC cell (dimension 5cm x 5cm) operated with pulverised charcoal fuel at 850 °C before (squares) and after (triangles) 12 hours stability test

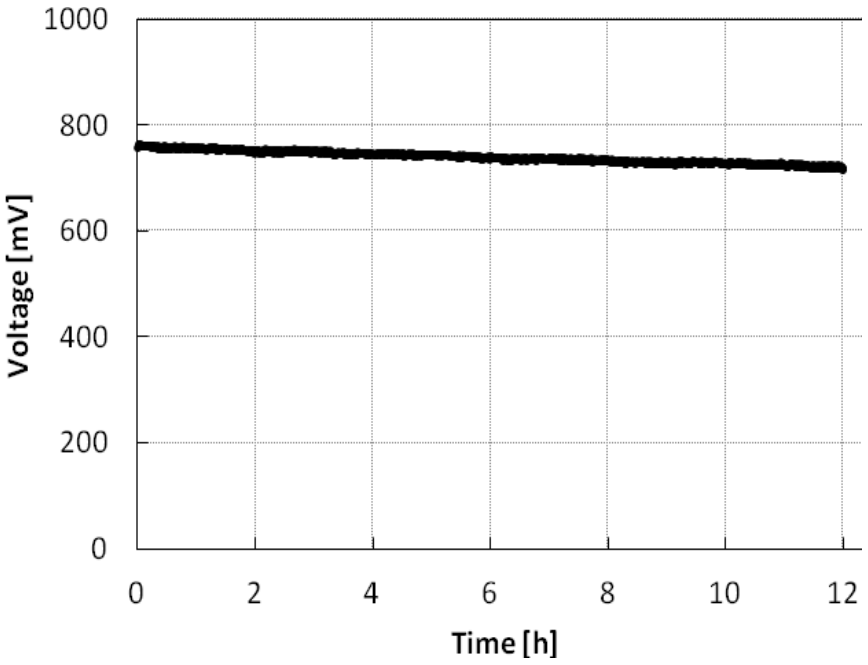


**Figure 9.** Dependence of the cell voltage on the time of loading (constant current load = 47 mA/cm$^2$ during 12 h). Other conditions as in Fig.8.

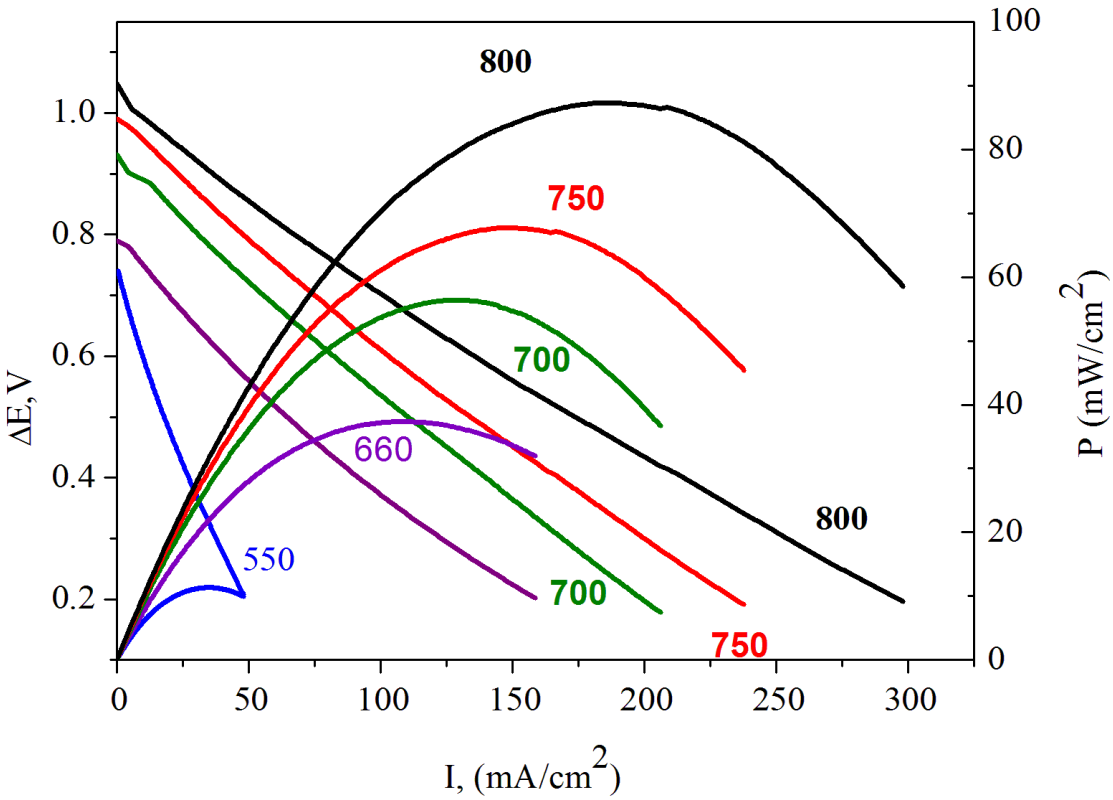


**Figure 10.** Families of dependences Δ*E* vs. *I* and *P* vs. *I* determined for the 2 cm$^2$ (a) type DC-SOFC. $CO_2$ atmosphere over the fuel (Charcoal B)

The additional experiments were performed with the 2 $cm^2$ type (a) fuel cells under $CO_2$ atmosphere in anodic compartment. In these conditions, $CO_2$ reacts with carbon, forming CO (reaction 3). CO, produced this way, improved performance of the cell by participation in reaction 2.

The families of Δ*E-I* and *P-I* curves are presented in Fig.10. As can be seen, the current and power densities were higher than those determined for the charcoals under Ar (Fig.8b). With $CO_2$ over Charcoal B, the maximum power density $P_{max}$ = 90 mW/$cm^2$ was reached in comparison to $P_{max}$ = 70 mW/$cm^2$ obtained with Ar in the anodic compartment. Moreover, the cell performance improved when the flow rate of $CO_2$ was increased. These observations clearly indicated that CO produced in reaction 3 had a significant contribution in the overall anodic reactions occurring in the DC-SOFC.

The additional experiments with the (e) type DC-SOFC were performed mainly for better understanding the mechanism of electro-oxidation of carbon originating from biomass. The fuel cell was not equipped with any porous anode deposited at the electrolyte and therefore the dominated electrode process was the direct electro-oxidation of carbon particles ($C + O^{2-} \rightarrow CO_2 + 4e^-$). For the cell (e) the ΔE-I and P-I curves (Fig.11) were recorded at a temperature of 700-850$^oC$. The current density and voltage increase vs. temperature.

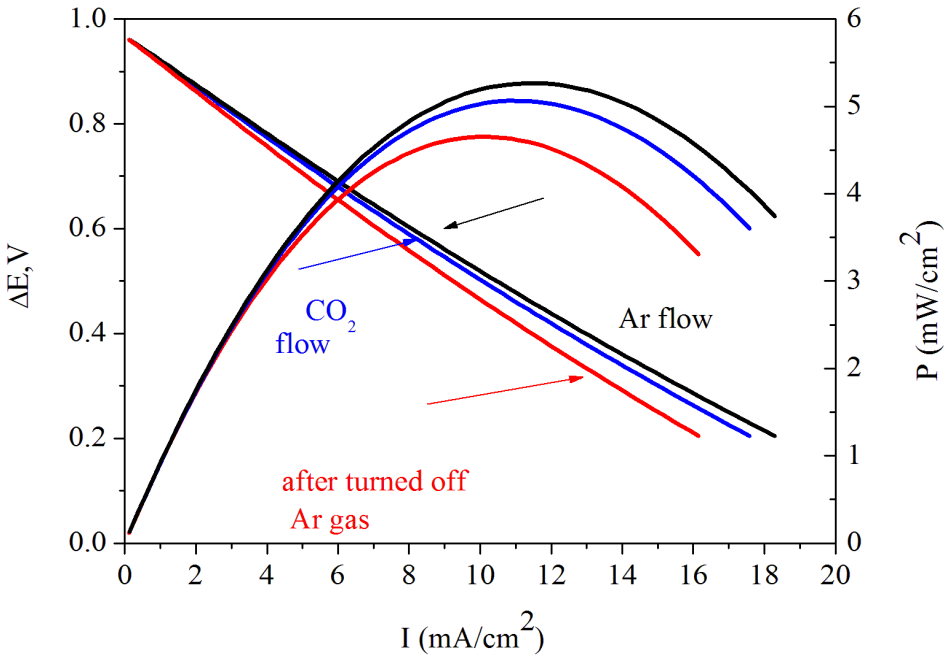


**Figure 11.** Families of dependences Δ*E* vs. *I* and *P* vs. *I* determined for the 2 $cm^2$ (a) type DC-SOFC at 800$^oC$ . Charcoal A was used as a fuel. Cell (e) without anode

The obtained values of current and power density are considerable lower than the case of cell (a) but in this case no dependence of current density and power density values in Ar or $CO_2$ gas atmosphere was noticed. As can be seen in Fig.12, the current densities slowly increased in the first 30 minutes, then rather stabilized in the next 10 hours.

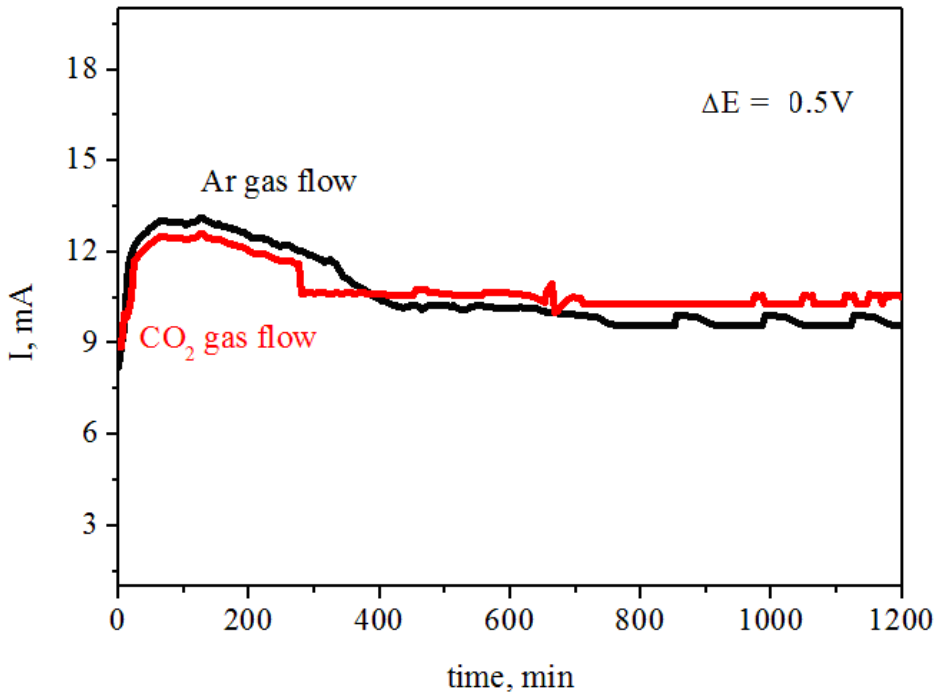


**Figure 12.** The dependences of the current density on time of loading (constant voltage $\Delta E$ = 0.5 V) for various atmospheres over the fuel (e) type of DC-SOFC) with no anode material deposited on the 8YSZ electrolyte. Temperature 800°C.

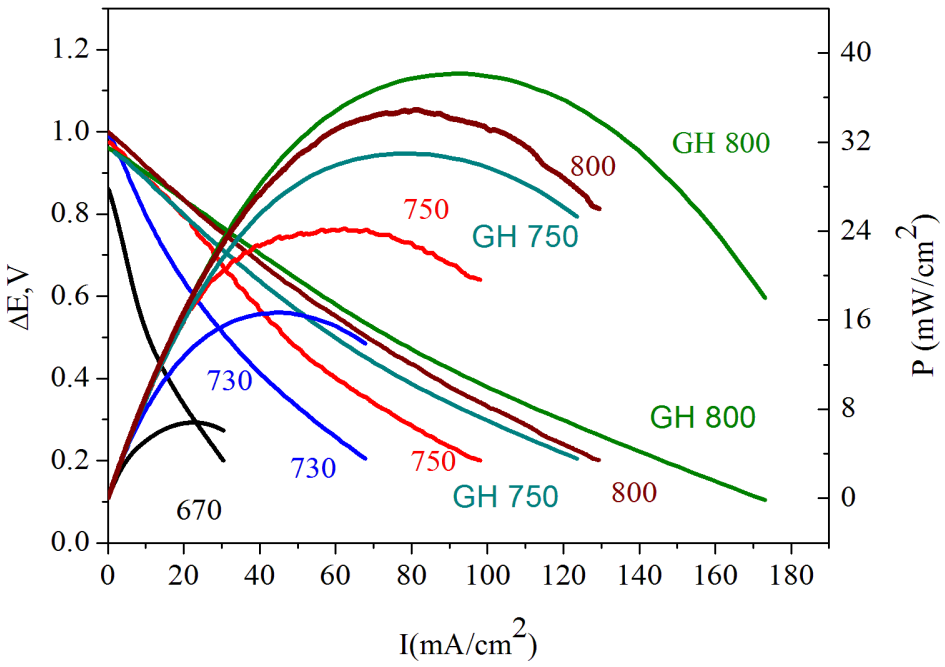


**Figure 13a.** Families of dependences $\Delta E$ vs. $I$ and $P$ vs. $I$ determined for the 2 cm$^2$ type DC-SOFC. Ar atmosphere over the fuel. For comparison data for the same cell fed with graphite powder (GH) was also added.

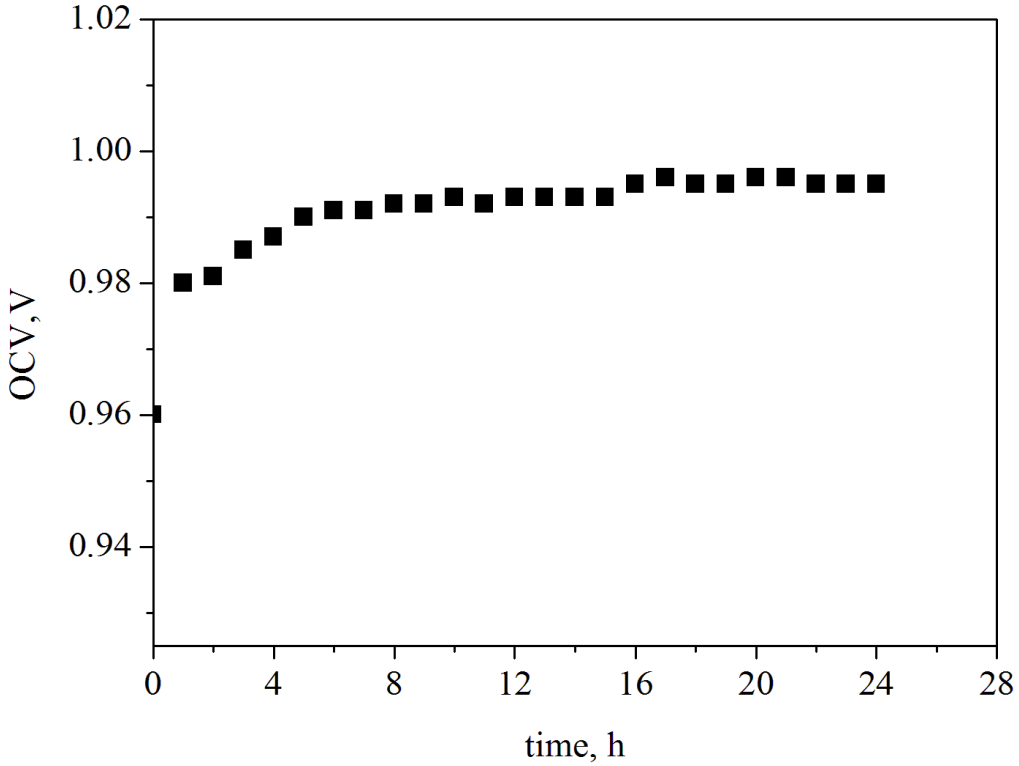


**Figure 13 b.** The OCV dependence vs. time at temperature 730$^{o}$C

One of the main strategies for developing DC-SOFCs regards the utilization of cheap wood-biomass waste as fuel. Typical $\Delta E$ vs. $I$ and $P$ vs. $I$ dependencies, recorded for Carbon C (wood chips pyrolysed in-situ) in the (a) type DC-SOFC, are shown in Fig.13a. As can be seen, the OCV approaches 0.95-1.00 V in the temperature range of 700-850$^{O}$C, close to the voltage of the DC-SOFC supplied with (Carbons A and B). The time dependence of OCV vs. time at 730$^{O}$C is presented in Fig.13b.

The OCV reached stable value after 5 minutes and was held for the whole duration of the over-six-hour experiment. The current and power densities acquired from the cell increased with the temperature up to ca. 35 mW/cm$^{2}$. These current and power densities were lower in comparison to these for the DC-SOFC fed with commercial Charcoals A and B but similar as in the case of pure graphite fuel *(GH*). The optimizing pyrolysis conditions of waste wood in situ DC-SOFC should be performed to improve the performance of the DC-SOFC.

*3.2.3. Electrochemical performance of the DC-SOFC with new oxide anode*

The development of new anode materials with desired physicochemical properties is an important issue for commercialization of the DC-SOFC fueled with biomass-derived carbon fuels. The oxide anode materials should have high catalytic activity and selectivity for carbon oxidation, sufficient oxygen non-stoichiometry, rapid oxygen chemical diffusion, wide thermodynamic stability

window to withstand reducing environment and sufficient electronic conductivity. Some perovskite groups of anode materials such as $La_{0.4}Sr_{0.6}Co_{0.2}Fe_{0.8}O_{3\pm\delta}$ and Fe –doped $SrTiO_3$ were proposed as suitable anode materials for the DC-SOFC [41,42].

On the other hand, cermetallic composites such as Cu-Ni-YSZ and Fe-Ni-GDC seem to be still promising materials for these applications [43-45]. In this work, Ni-GDC, $(Ni_{0.9}Fe_{0.1})$-GDC and $La_{0.8}Ca_{0.1}Sr_{0.1}CrO_3$ (LCCr) were tested as anode materials for the DC-SOFC (types (b), (c) and (d)) fed with charcoal as a solid fuel.

The families of dependences $\Delta E$ vs. $I$ and $P$ vs. $I$ recorded at 800$^{o}$C for these fuel cells are presented in Fig.14 a. The current and power densities acquired from the DC-SOFC with the anodes made of Ni-GDC and $(Ni_{0.9}Fe_{0.1})$-GDC cermets, were higher compared to these acquired from the DC-SOFC with the Ni-YSZ anode. The maximum power densities were 62, 78 and 109 mW/cm$^2$ for the DC-SOFC with the Ni-YSZ, Ni-GDC and (Ni-Fe)-GDC anodes, respectively. The data was obtained for Charcoal A under an Ar atmosphere.

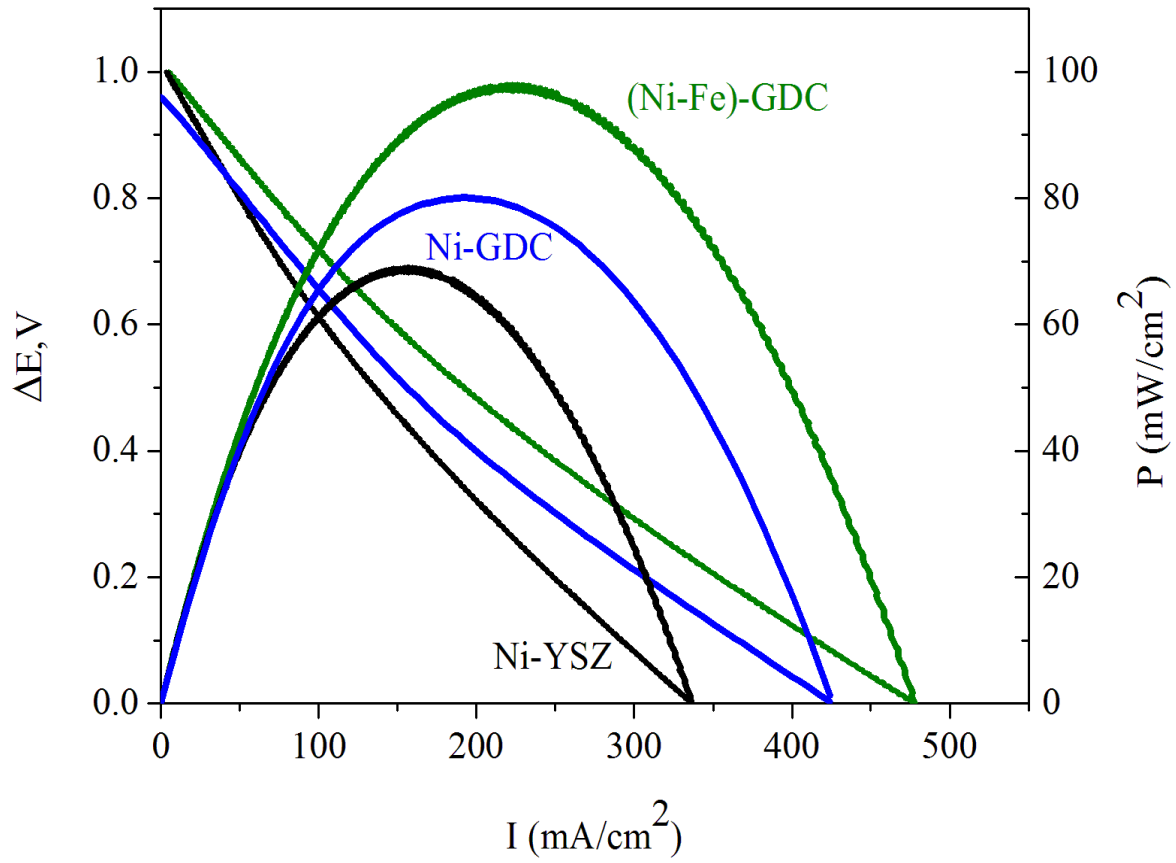


**Figure 14a.** Families of dependences $\Delta E$ vs. $I$ and $P$ vs. $I$ determined for the 2 cm$^2$ DC-SOFC with Ni-YSZ, Ni-GDC and (Ni-Fe)GDC cermetallic anodes (cell types (a), (b) and (c), respectively. Ar gas atmosphere over the fuel. Temperature: 800°C.

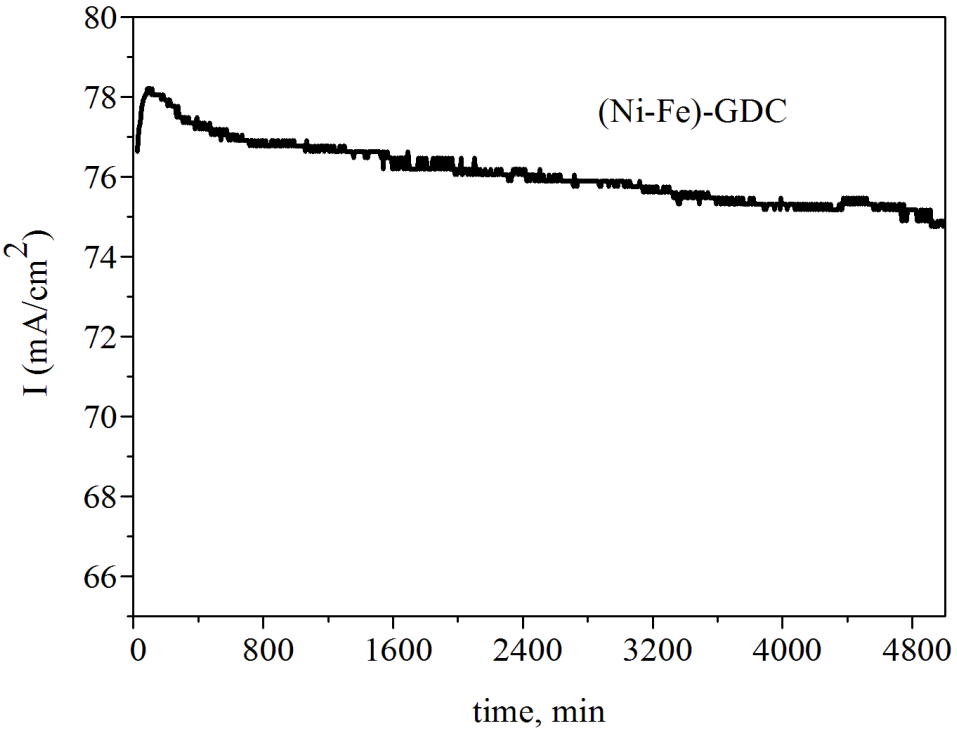


**Figure 14b.** The dependences of the current density on time of loading (constant voltage $\Delta E$ = 0.5 V) for Ar gas atmosphere over the fuel (c) type of DC-SOFC. Temperature 800°C.

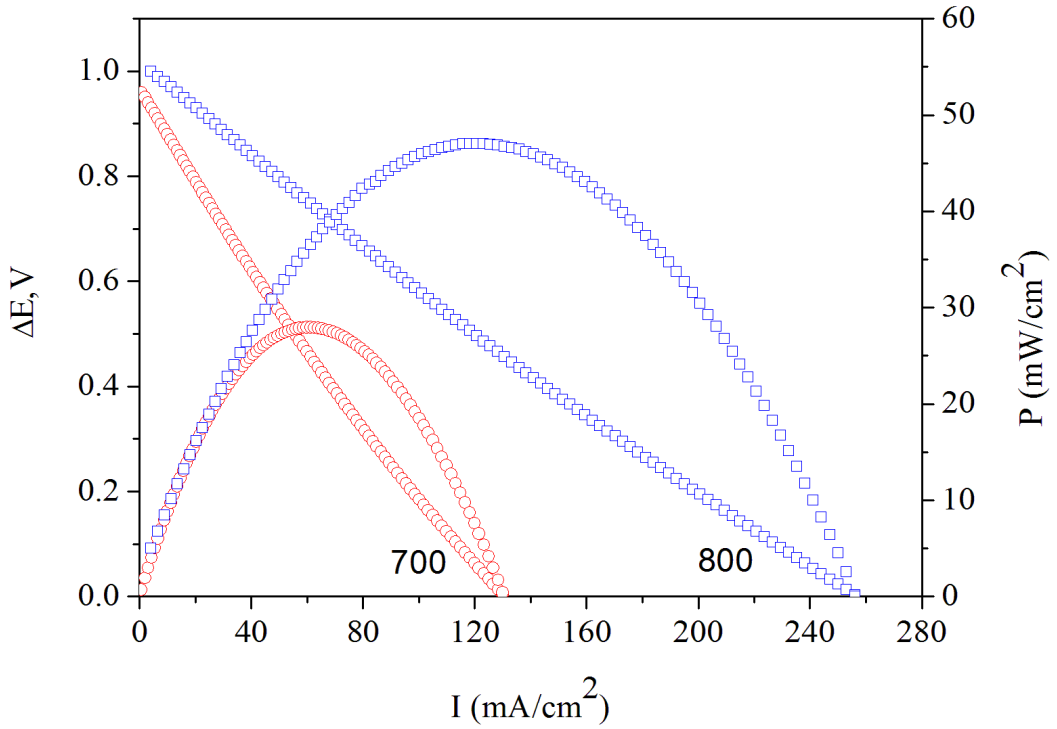


**Figure 15.** Families of dependences $\Delta E$ vs. $I$ and $P$ vs. $I$ determined for the 2 cm$^2$ (d) type DC-SOFC with $La_{0.8}Ca_{0.1}Sr_{0.1}CrO_3$ anode, Ar gas atmosphere over the fuel. Temperature: 700°C and 800°C

The GDC electrolyte shows the higher ionic conductivity and better catalytic properties for the carbon direct and indirect oxidation then YSZ. This behavior of GDC is due to the fact that ceria has two stable oxidation states $Ce^{3+}$ and $Ce^{4+}$, hence addition of $Gd^{3+}$ to ceria lattice enhanced the oxygen mobility by creating oxygen vacancies. As a consequence, $CeO_2$-based materials show better ability to oxidize carbon to CO or/and $CO_2$, than ,for example, Ni-YSZ. It was already reported that electrodes made of Ni-GDC cermets are effective anodes preventing coke build–up when low humidified $CH_4$ fuels are used to feed the direct $CH_4$-SOFC [46,47]

At higher temperatures, the higher oxygen mobility in ceria promotes the mechanism of carbon removal by oxidation to CO or/and $CO_2$. The performance of these materials can be additionally improved by uniform dispersing nobel-metal catalysts as Ru and Pd at their surface [48] Another approach to improve the anode performance is the addition of other transition metals such as Fe, Cu and Co into Ni to form bimetallic or trimetallic alloys [49,50]

Ni-Fe bimetal mixed with YSZ, SDC or $(La,Sr)(Ga,Mg)O_3$ demonstrated to possess a noticeably improved performance over Ni cermet anodes. Although the steam reforming activity of $CH_4$ at the Fe-YSZ is much lower than at Ni-YSZ at open circuit voltage, the Fe-YSZ anode exhibited excellent resistance against coking Iron is also considered to be a promising, inexpensive catalyst for the Boudouard reaction 3 to accelerate formation of CO [51]

Y.Tang and J.Liu [52] investigated the performance of the DC-SOFC with the Ag-GDC anode fed with composite fuel consisting of carbon powder and Fe catalyst. They found that the addition of iron into carbon powder enhances rate of the Boudouard reaction. The additional amount of CO led to a significant increase of current and powder densities produced by the DC-SOFC. Therefore, the bimetallic anode (Ni-Fe)-GDC is believed to be more suitable than Ni-GDC for utilization of charcoals in the DC-SOFC. The experimental results presented in Fig. 14a justified the above conclusions. The time dependence of current density (I) under polarization at – 0.5 V was also presented in Fig. 14 b. A small increase in the first stage polarization (60 min) and a slightly slow decrease were observed for (Ni-Fe)-GDC anode material after 60h of long-cast time experiment.

The application of perovskite oxides as anode materials for the DC-SOFCs seems to be a potentially attractive option too. A. Kulkarni et al. [53] presented the preliminary characteristics of the DC-SOFC with 20GDC electrolyte and LSCF anode. The current and power densities produced by this cell were significantly higher than those produced by the DC-SOFC with the Ni-YSZ cermet anode. In this work, we also investigated the effect of $La_{0.8}Sr_{0.1}Ca_{0.1}CrO_3$ anode on the DC-SOFC performance. The dependencies $\Delta E$-$I$ and $P$-$I$ for the (d) type DC-SOFC in the temperature range 700 to 800°C is presented in Fig. 15. As can be seen, the current and power densities increased with increase of temperature. The maximum power of the cell was slightly lower in comparison to the DC-SOFC with the Ni-YSZ anode. We expect that optimizing the microstructure and porosity of the anode material will reduce anode polarization.

## 4. CONCLUSIONS

1. Three different biomass products, namely charcoal powder (supplied by Merck Germany), Carbo medicinalis (commercial product supplied by Gryfskand, Poland) and wood-chips

produced from a beech wood and pyrolysed in situ in the fuel cell, were tested as potential fuels for the direct carbon fuel cell with solid oxide electrolyte.

2. The samples of biomass fuels were examined by ultimate analysis, XRD, XPS/ESCA spectroscopy and thermal analysis (DTA/DSC-TG). These studies showed that the fuels under studies have large surface area, produced very little ash when burned, contained no mercury, almost no sulphur and low nitrogen. The analyses confirmed the presence of graphite-like phases of carbon, although its structure was highly defected and contained amorphous C.

3. The electrochemical oxidation of biomass fuels (charcoals) were investigated using five types of small solid oxide fuel cells (button-size with ca. 2 $cm^2$ active surface area) with the same electrolyte (8YSZ) and cathode (LSM-GDC) materials, which varied only in composition of the anode material. Some experiments were also performed with the larger (5 cm x 5 cm) DC-SOFC. These experiments confirmed that charcoals, also including wood-chips pyrolysed in situ, are suitable and attractive fuels for the DC-SOFC providing sufficiently high power density (50-100 $mW/cm^2$) under load.

4. The experiments with different atmospheres (Ar, $N_2$ and $CO_2$) over the charcoal fuel as well as these with the fuel cells without or with various anodic materials, revealed that CO produced in the Boudouard reaction 3 had significant contribution in the overall anodic reactions occurring in the DC-SOFC.

**5.** On the basis of these experiments it was concluded that employment of anode materials with better abilities of C and CO oxidation than currently used Ni-YSZ, would improve the performance of the DC-SOFC in long duration of loading. The tests of fuel cells with Ni-GDC, (Ni-Fe) cermetallic and LCCr oxide anodes confirmed the above conclusion.

## References

1. P. Carneiro, P. Ferreira, *Renew Energ*, 44 (2012)17
2. N. Kautto, P. Peck, *Renew Energ*, 46 (2012) 23
3. J.V Dam, A.P.C. Faaij, I. Lewandowski, G. Fischer, *Biomass Bioenerg*, 31(2007) 345
4. J. Heinimö, M. Junginger, *Biomass Bioenerg*, 33 (2009) 1310
5. L.S. Esteban, J.E. Carrasco, *Biomass Bioenerg* 35 (2011)S21
6. J.G. Rogers, J.G. Brammer, *Biomass Bioenerg* 33 (2009) 1367.
7. R. Toonssen, N. Woudstra, A. H.M. Verkooijen, *J Power Sources*, 194 (2009) 456
8. P. Leone, A. Lanzini, M. Santarelli, M. Calì, F. Sagnelli, A. Boulanger, A. Scaletta, P. Zitella, *J Power Sources* 195 (2010) 239
9. C. Tomasi, M. Baratieri, B. Bosio, E. Arato, P. Baggio, *J Power Sources* 3 (2006) 765
10. M. J. Antal, M. Grønli *Ind. Eng. Chem. Res.* 42 (2003)1619
11. J.G. Hernandez, I. Hernandez-Calderon, C. A. Luengo, R. Tsu, *Carbon* 20 (1982) 201
12. N.Cao, H. Darmstadt, F. Soutric, Ch. Roy, *Carbon* 40 (2002) 471
13. S. V. Vassilev, D. Baxter, L.K. Andersen, Ch. G. Vassileva, T.J. Morgan, *Fuel* 94 (2012) 1
14. M. Cassir, S.J. McPhail, A. Moreno, *Int J Hydrogen Energ* 37 (2012) 19345
15. L. Jia, Y. Tian, Q. Liu, Ch. Xia, J. Yu, Z.Wang, Y. Zhao, Y. Li, *J Power Sources* 195 (2010) 5581
16. N.J. Cherepy, NJ Krueger, R.Fiet, K. J Jankowski, *J Electrochem Soc* 2005 (152) A80
17. A.L. Dicks, *J Power Sources* 156 (2006) 128
18. S.L. Jain, J.B.Lakeman, K. D. Pointon, R. Marshall, J.T. Irvine, *Energy Environ Sci* 2 (2009) 687
19. C.Jiang, A.D, Bonaccorso, T.S Irvine. *Energy Environ Sci* 5 (2012) 6973

20. M. Dudek, P. Tomczyk, K.L. Juda, R.Tomov, B.A.Glowacki , S. Batty, P. Risby, R.Socha, *Int. J. Electrochem. Sci* 7 (2012) 6704
21. R. Liu, Ch. Zhao, J. Li, F. Zeng, S. Wang, T. Wen, Z.Wen, *J Power Sources* 195 (2010) 480
22. Y.Wu, Ch.Su, Ch.Zhang, R.Ran, Z.Shao, *Electrochem. Comun11*(2009)1265
23. C. Jiang, J. T.S. Irvine, *J Power Sources* 196 (2011) 7318,
24. M. Dudek, P. Tomczyk, *Catal. Today* 176 (2011) 388
25. J. F. Moulder, W. F. Stickle, P. E. Sobol, and K. Bomben (J. Chastain, editor), Handbook of X-ray Photoelectron Spectroscop 2nd ed. Perkin-Elmer Corporation (Physical Electronics), 1992 (2nd edition).
26. E.Z. Kurmaev, S.N. Shamin, K.M. Kolobova, S.V. Shulepov, *Carbon* 24 (3) 1986, 249-253
27. J.A. Leiro, M.H. Heinonen, T. Laiho, I.G. Batirev, *J. Electron Spectrosc. Relat. Phenom*. 128 (2003) 205
28. G. A. Zickler, B.Smarsly, N. Gierlinger, H. Peterlik, O.Paris, *Carbon* 44 (2006) 3229
29. A. K. Kercher, D. C. Nagle, *Carbon* 41 (2003) 15
30. Lu, C. Kong, V. Sahajwalla, D. Harris, *Fuel* 81 (2002) 1215.
31. Ch. Li, Yixiang Shi, N. Cai, *J Power Sources* 196 (2011) 4588
32. A.Gunji , C.Wen, J.Otomo, T.Kobayashi, K.Ukai ,Y. Mizutani,. *J Power Sources* 131 (2004)285
33. T. Namioka, T. Naruse, R. Yamane, *Int J Hydrogen Energ* 36 (2011) 558
34. Chun, J.D.Mumford, T.Ramanarayanan, , *J Electrochem Soc* 147 (2000) 3680
35. S.P. Jiang, S.H.Chan, *J. Mater. Sci.* 39 (2004) 4405
36. T.Horita, N.Sakai, T.Kawada, H. Yokokawa, M Dokiya, *J Electrochem Soc* 142 (1995)2621
37. T. M. Gür and R. A. Huggins, *J Electrochem.Soc*. 139 (1992) L95
38. Ch. Li, Y.Shi, N.Cai, *J Power Sources* 196 (2011) 754
39. T. M. Gür, *J Electrochem. Soc*. 157 (2010) B571
40. P. Tomczyk, *J. Power Sources*, 160 (2006) 858
41. A. Kulkarni, S. Giddey, S.P. Badwal, *Solid State Ionics* 194 (1) 2011, 46
42. J.P Kim, H-K Choi, Y.-JChang, C. H Jeon, *Int J Hydrogen Energ* 37 (2012) 11401
43. C.J.Fu, S.H.Chan, X.M. Ge, Q.L. Liu, G.Paściak, *Int J Hydrogen Energ* 36 (2011) 1327
44. R.J Gorte ,V.J Vohs. *J Catal* 216 (2003) 477
45. W. Wang, S. P. Jiang, A. I. Yoong T., L.Luo, *J Power Sources* 159 (2006) 68
46. K.Cheng, H.Chen, W.Wenig, C.Song, P.Du, G.Shen, G.Hun, *J Alloy Comp* 541 (2012) 65
47. Y.M. Choi, Ch. Compson, M.C. Lin, *J Alloy Comp* 427 (2007) 25
48. R. Kikuchi , N. Koashi, T. Matsui, K. Eguchi, T. Norby , *J Alloy Comp* 334 (2002) 299
49. J. Ding, J. Liu ,W.Guo, *J Alloy Comp* 480 (2009) 286-290
50. B. Liang, T. Suzuki, K. Hamamoto, T. Yamaguchi, H. Sumi, Y. Fujishiro, B. J. Ingram, J.D. Carter, *J Power Sources* 202 (2012) 225
51. Ch. Sun , U. Stimming, *J Power Sources* 171 (2007) 247
52. Y. Tang, J. Liu, *Int J Hydrogen Energ* 35 (2010) 11188
53. A. Kulkarni , F.T. Ciacchi, S. Giddey, C. Munnings, S.P.S. Badwal, , J.A. Kimpton, D. Fini, *International Int J Hydrogen Energ* 37 (2012) 19092